Optimal Control in Blood Flow Simulations

Telma Guerra[a], Jorge Tiago[b], Adélia Sequeira[b,*]

[a]*Department of Mathematics and Management, Escola Superior de Tecnologia do Barreiro (IPS), Rua Américo da Silva Marinho, 2839-001 Lavradio, Lisbon, Portugal and CMA, FCT-UNL*
[b]*Department of Mathematics and CEMAT, Instituto Superior Técnico, Av. Rovisco Pais, 1049-001 Lisbon, Portugal*

Abstract

Blood flow simulations can be improved by integrating known data into the numerical simulations. Data assimilation techniques based on a variational approach play an important role in this issue. We propose a nonlinear optimal control problem to reconstruct the blood flow profile from partial observations of known data in idealized 2D stenosed vessels. The wall shear stress is included in the cost function, which is considered as an important indicator for medical purposes. To simplify we assume blood flow as an homogeneous fluid with non-Newtonian behavior. Using a Discretize then Optimize (DO) approach, we solve the nonlinear optimal control problem and we propose a weighted cost function that accurately recovers both the velocity and the wall shear stress profiles. The robustness of such cost function is tested with respect to different velocity profiles and degrees of stenosis. The filtering effect of the method is also confirmed. We conclude that this approach can be successfully used in the 2D case.

Keywords: Optimal Control, Non-Newtonian fluids, Data Assimilation

1. Introduction

Nowadays medical researchers, bioengineers and numerical scientists join efforts and work together with the purpose of providing numerical simulations

*Corresponding author
Email addresses: telma.guerra@estbarreiro.ips.pt (Telma Guerra), jftiago@math.ist.utl.pt (Jorge Tiago), adelia.sequeira@math.ist.utl.pt (Adélia Sequeira)

of the human cardiovascular system in healthy and unhealthy conditions. This multidisciplinary collaboration offers not only an exchange of knowledge between those communities but also an exchange of data information that can be used in the numerical simulations to predict the blood flow behavior under healthy or diseased conditions.

The progress in medical imaging techniques, blood flow modelling, and computational techniques can be joined together to obtain patient specific simulations. When such tools are available to the medical community, the advantages in therapy prediction, training and expenses reduction can be very significant. Data information must be included in the numerical simulations to obtain accurate results. These techniques are known in the literature as Data Assimilation (DA) techniques. They have been widely used in some engineering fields, like geophysics and meteorology, but recent work ([9, 10]) has shown that DA can also be successfully used to simulate blood flow problems.

One of the most frequent diseases of the cardiovascular system, is atherosclerosis, which gives rise to a stenosis of the blood vessels, by partially obstructing them. This reduction in the vessel diameter changes in particular the mechanical behavior of the blood circulation. Although not yet fully understood, it is already known that hemodynamical characteristics, like the shear stress exerted by the blood flow on the vessel walls, can affect the progression of this and of other pathologies (see [7, 19, 4]).

In normal situations the blood flow has a Newtonian behavior in most parts of the arterial system. In fact, non-Newtonian effects are mostly observed in the nervous system, in the case of blood vessel aneurysms or downstream a stenosis related to the existence of atherosclerosis. In such cases it is important the study of non-Newtonian blood flow behavior, including shear-thinning viscosity, thixotropy, viscoelasticity, and the yield stress. This behavior is related to the properties of red blood cells, namely its tendency to form tridimensional structures at low shear rates and to disaggregate and align in blood flow direction at high shear rates ([21]).

In this paper we focus on the above aspects of blood flow. In this sense, we propose and validate a DA method, based on a variational approach ([9]), to numerically reconstruct the blood flow in 2D idealized stenosis, governed by a generalized Newtonian model with shear-thinning viscosity. In the DA method we take into account the Wall Shear Stress (WSS) and we verify that this leads to a better precision in a posteriori measurements. We validate the robustness of the method with respect to the stenosis degree and to different

flow profiles. Additionally, we verify the filtering effect of the DA process.

The paper is organized as follows. Section 2 is devoted to the mathematical model that will be used later in the numerical simulations. In Section 3 we describe the DA procedure as a variational frame, which is our choice for DA implementation and we state the derived control problem formulation. Section 4 is essentially devoted to the discretization of the optimal control problem using DO approach. Numerical results related to the choice and robustness of the cost function parameters are reported in Section 5. Finally, we summarize our conclusions in Section 6.

2. Dynamic equations and viscosity models

Along this work, the blood flow is modeled as an incompressible and laminar fluid whose dynamic equations derive from classical mechanics principles: the conservation of mass and of linear momentum. These equations describe the fluid motion in an domain of interest $\Omega \subset R^2$ and can be written as

$$\begin{cases} \rho\left(\frac{\partial \mathbf{y}}{\partial t} + (\mathbf{y}\cdot\nabla)\mathbf{y}\right) - div\,(\tau(D\mathbf{y})) + \nabla p = \mathbf{f} & \text{in } \Omega \\ div\,\mathbf{y} = 0 & \text{in } \Omega \end{cases} \tag{1}$$

with suitable boundary conditions. The control and state variables are constrained to satisfy a system with shear dependent viscosity which decreases with increasing shear rate (shear-thinning fluid). The unknowns are the velocity field $\mathbf{y}$ and the pressure p. The density of the fluid is represented by ρ and $\mathbf{f}$ is the given body force. The viscous stress tensor is represented by

$$\tau = 2\mu(\dot{\gamma})D\mathbf{y}$$

where μ is the viscosity, $\dot{\gamma}$ is the shear rate given by

$$\dot{\gamma} = \sqrt{\frac{1}{2}(\nabla\mathbf{y} + (\nabla\mathbf{y})^T) : (\nabla\mathbf{y} + (\nabla\mathbf{y})^T)} = \sqrt{2}|D\mathbf{y}|\,,$$

and D is the strain tensor

$$D\mathbf{y} = \frac{1}{2}(\nabla\mathbf{y} + (\nabla\mathbf{y})^T)\,,$$

that is, the symmetric part of the velocity gradient.

For a Newtonian flow, μ is a constant and τ is a linear function depending on $D\mathbf{y}$. This property is not verified when the fluid has a non-Newtonian

flow behavior and μ is a nonlinear function of the stress tensor. This leads to difficulties in the treatment of the non-linearities in addition to the convective term that has also a nonlinear nature.

Here we compare blood flow simulations for a 2D generalized Newtonian model with shear-thinning viscosity in the sationary case.

Viscosity functions can be written in the general form

$$\mu(\dot{\gamma}) = \mu_\infty + (\mu_0 - \mu_\infty)F(\dot{\gamma}) \tag{2}$$

where μ_0 and μ_∞ are the asymptotic viscosity values at zero and at infinite shear rates, respectively, and $F(\dot{\gamma})$ is a bounded function depending on the shear rate. The function F is such that

$$\lim_{\dot{\gamma}\to 0} F(x) = 1 \quad \text{and} \quad \lim_{\dot{\gamma}\to +\infty} F(x) = 0.$$

Different choices of F correspond to different blood flow models. The choice of the correct viscosity blood is important to obtain accuracy in blood flow simulations and the viscosity parameters related to each model have to be chosen according to the specific model and taking into account physical parameters like the temperature, hematocrit (percentage of red blood cells per unit volume) and the healthy or unhealthy state of the individual donor ([21, 24]).

In [12], the authors used known estimates to convert data and obtained realistic viscosity values at 37C. Comparing data for different viscosity models, they obtained the constants for each one using nonlinear least squares fitting of the viscosity data. Despite the absence of data for μ_0, the authors concluded that the Carreau and the Cross models fit very well the experimental data.

Based on their conclusions, for the $2D$ stenosis case, we considered

$$F(\dot{\gamma}) = \frac{1}{(1 + (\lambda\,\dot{\gamma})^b)^a}\,,$$

with the parameters $a, b, \lambda > 0$. Hence (2) becomes

$$\mu(\dot{\gamma}) = \mu_\infty + \frac{\mu_0 - \mu_\infty}{(1 + (\lambda\,\dot{\gamma})^b)^a}\,, \tag{3}$$

which is usually known as the generalized Cross model.

3. The DA method

In this section we describe our approach to the DA problem. The main goal is to obtain numerical solutions for problem (1) which coincide, within a certain error, to observed data measured in certain parts of the domain. Different techniques may be used for this purpose, namely the so called variational approach, and, at the discrete level, matrix updating or domain splitting. In [11] the variational approach gives better results than the two others.

The variational approach is based on the assumption that we are free to adjust or control some of the model parameters and chose among the corresponding solution, according to some criteria. In the simplest frame such criteria corresponds to the difference

$$\int_{\Omega_{part}} |\mathbf{y} - \mathbf{y}_d|^2 \, dx$$

between the obtained solution $\mathbf{y}$ and the data $\mathbf{y}_d$ measured over a subdomain Ω_{part}. By taking the adjustable parameters as a control function $\mathbf{u}$ defined on Ω_c, possibly different from Ω_{part}, we are then facing an optimal control problem which also corresponds to an inverse problem. It is known that, when dealing with linear models, the possible ill-posedness (non uniqueness) of such inverse problem can be avoided by adding to the criteria a regularizing term like

$$\int_{\Omega_c} |\mathbf{u}|^2 \, dx \quad \text{or} \quad \int_{\Omega_c} |\nabla \mathbf{u}|^2 \, dx.$$

Using such type of cost functions allows to prove, within certain assumptions, the uniqueness of solution for the corresponding optimal control problem.

Here we assume that the 2D domain Ω represents an artery truncated by two artificial boundaries Γ_{in} and Γ_{out}, the inlet and outlet respectively, as represented in Figure 1.

The control function corresponds to the inlet velocity field profile. We also assume that the data corresponds to the velocity observed in $\Omega_{part} \subset \Omega$. Additionally, we can assume to know the WSS in a certain part of the boundary Γ_{wall}. In fact, as mentioned in Section 1, the WSS is an important indicator for monitoring certain pathologies. Therefore, it is desirable that the DA

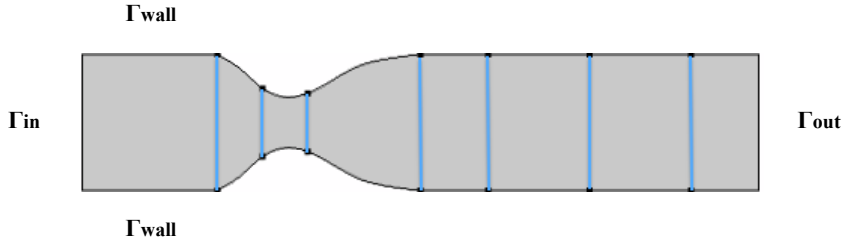

Figure 1: Computational domain Ω.

method can accurately reconstruct the desired WSS. In this sense we also include the difference

$$\int_{\Gamma_{wall}} |w - w_d|^2$$

between the obtained WSS magnitude w and w_d, the registered WSS magnitude. Note that the WSS is the tangential component of the stress exerted by the fluid in the vessels wall and is given by

$$WSS = \sigma_n - (\sigma_n \cdot \mathbf{n})\mathbf{n}\,, \tag{4}$$

where $\mathbf{n}$ is the outward normal to the wall surface and $\sigma_n = \sigma\mathbf{n}$ is often called the normal component of the stress tensor σ. Assuming $\sigma = p\mathbf{I} - \tau$, (4) can be written as

$$WSS = \mu(\nabla\mathbf{y} + (\nabla\mathbf{y})^T)\mathbf{n} - \mu[((\nabla\mathbf{y} + (\nabla\mathbf{y})^T)\mathbf{n}) \cdot \mathbf{n}]\mathbf{n}\,. \tag{5}$$

The DA method consists in solving the optimal control problem

$$\min_u \mathbf{J}(\mathbf{y}, \mathbf{u}) = w_1 \int_{\Omega_{part}} |\mathbf{y} - \mathbf{y}_d|^2\, dx + w_2 \int_{\Gamma_{wall}} |w - w_d|^2\, dx + w_3 \int_{\Gamma_{in}} |\nabla\mathbf{u}|^2\, dx \tag{6}$$

subject to

$$\begin{cases} -div\,\tau + \rho(\mathbf{y}\cdot\nabla)\mathbf{y} + \nabla p = \mathbf{f} & \text{in } \Omega \\ div\,\mathbf{y} = 0 & \text{in } \Omega, \\ \mathbf{y} = 0 & \text{on } \Gamma_{wall} \\ \mathbf{y} = \mathbf{u} & \text{on } \Gamma_{in} \\ -\sigma\mathbf{n} = 0 & \text{on } \Gamma_{out}. \end{cases} \tag{7}$$

The weights w_1, w_2 and w_3 should be chosen in such a way that problem (6 - 7) admits a solution (preferably unique).

As far as we know, the existence of a solution to problem (6 - 7) has not been studied, even for the quadratic cost functional obtained by taking $w_2 = 0$. In fact, optimal control problems for non-Newtonian fluids have been studied only very recently. For the two-dimensional steady case we mention [5], where boundary control of quasilinear elliptic equations are considered, and [6, 22] both for distributed control. For the two-dimensional unsteady case, we refer to [23], and to [18] for three-dimensional coupled modified Navier-Stokes and Maxwell equations. Furthermore, for distributed control on three-dimensional domains we cite [1] and [16]. None of the cited authors focused on the boundary control problem for the nonlinear system (7).

In spite of lacking an appropriate theoretical frame, we assume enough regularity on the problem variables and we propose a numerical approach to solve the problem. This will be the subject of next section.

4. Discretization of the main problem

The numerical solution of an optimal control problem can be obtained either by the Discretize then Optimize (DO) or the Optimize then Discretize (OD) approaches. There is still some controversy concerning the performance of each one of those approaches. Here we follow the work [9] where the DO approach is used (see, for instance, [17] for some comments on this issue).

The DO approach consists in first discretizing the optimal control problem and then solve the finite dimensional optimization problem resulting from the discretization. For the first step we use typical FEM. We first address the weak formulation of (1) in the steady case.

Let us assume that we are looking for $\mathbf{y} \in \mathbf{H}^1(\Omega)$ and for $p \in \mathbf{L}^2(\Omega)$. We consider $\mathbf{V} = \{\mathbf{v} \in \mathbf{H}^1(\Omega) : \ \mathbf{v}|_{\partial\Omega_D} = 0\}$, where $\partial\Omega_D = \Gamma_{in} \cap \Gamma_{wall}$, and $\mathbf{Q} = \mathbf{L}^2(\Omega)$ as the spaces of test functions corresponding to $\mathbf{y}$ and p, respectively. Multiplying (1) by suitable test functions and integrating by parts we obtain

$$\begin{cases} \int\limits_{\Omega} \tau(D\mathbf{y}) : \nabla\mathbf{v} + \int\limits_{\Omega} (\rho(\mathbf{y}\cdot\nabla)\mathbf{y})\cdot\mathbf{v} - \int\limits_{\Omega} p\, div\, \mathbf{v} = \int\limits_{\Omega} \mathbf{f}\cdot\mathbf{v} \\ \int\limits_{\Omega} q\, div\, \mathbf{y} = 0 \end{cases} \tag{8}$$

for all $\mathbf{v} \in \mathbf{V}$ and $q \in \mathbf{Q}$.

Let us consider the finite dimensional subspaces $\mathbf{V}_h \subset \mathbf{V}$ and $\mathbf{Q}_h \subset \mathbf{Q}$ with $h > 0$, $dim(\mathbf{V}_h) = N_y$ and $dim(\mathbf{Q}_h) = N_p$. We then take the finite dimensional approximations

$$\mathbf{y}_h = \sum_{j=1}^{N_y} y_j\phi_j \in \mathbf{V}_h, \quad p_h = \sum_{k=1}^{N_p} p_k\psi_k \in \mathbf{Q}_h \tag{9}$$

where ϕ_j and ψ_k are the shape functions belonging to $\mathbf{V}_h$ and $\mathbf{Q}_h$ respectively. The coefficients y_j and p_k are unknown values to be determined.

Considering that the space of the shape functions coincides with the space of the test functions, we reach the following approximated problem: find $\mathbf{y}_h \in \mathbf{V}_h$ and $p_h \in \mathbf{Q}_h$ such that

$$\begin{cases} \int\limits_{\Omega} \tau(D\mathbf{y}_h) : \nabla\mathbf{v}_h + \int\limits_{\Omega} (\rho(\mathbf{y}_h\cdot\nabla)\mathbf{y}_h)\cdot\mathbf{v}_h - \int\limits_{\Omega} p_h\, div\, \mathbf{v}_h = \int\limits_{\Omega} \mathbf{f}\cdot\mathbf{v}_h, \\ \int\limits_{\Omega} q_h\, div\, \mathbf{y}_h = 0, \end{cases} \tag{10}$$

for all $\mathbf{v}_h \in \mathbf{V}_h$ and $q_h \in \mathbf{Q}$. If we choose $\mathbf{V}_h$ and $\mathbf{Q}_h$ compatible (see e.g. [8]) then it is possible to prove the existence of a solution of the approximated problem and to check that $(\mathbf{y}_h, p_h)$ converges to the solution $(\mathbf{y}, p)$ of (8).

Here we use the well known spaces corresponding to the Taylor-Hood elements ($P2$-$P1$), both for shape and test functions to built the finite element spaces $\mathbf{V}_h$ and $\mathbf{Q}_h$, respectively.

First, let us consider the convective term

$$\int\limits_{\Omega} (\rho(\mathbf{y}_h\cdot\nabla)\mathbf{y}_h)\cdot\mathbf{v}_h\,.$$

Replacing $\mathbf{y}_h$ by the corresponding finite approximation (9) and $\mathbf{v}_h$ by the test functions $\phi_i,\ i = 1...N_y$, we obtain

$$\int_\Omega \left[\left(\rho \sum_{j=1}^{N_y} y_j \phi_j \cdot \nabla \right) \sum_{k=1}^{N_y} y_k \phi_k \cdot \phi_i \right], \ i = 1...N_y \, .$$

This can be written as

$$\left(\sum_{j=1}^{N_y} y_j \sum_{k=1}^{N_y} y_k \int_\Omega (\rho \phi_j \cdot \nabla) \phi_k \cdot \phi_i \right)_{i=1...N_y} = \mathbf{G}(Y) Y,$$

where $Y = (y_1, ..., y_{N_y})^T$ and

$$\mathbf{G}(Y) = \sum_{k=1}^{N_y} y_k \int_\Omega (\rho \phi_j \cdot \nabla) \phi_k \cdot \phi_i \, .$$

We now turn our attention to the viscous stress tensor τ. The term we want to discretize is

$$\int_\Omega \tau(D\mathbf{y}_h) : \nabla \mathbf{v}_h$$

where the tensor is written as

$$\tau = 2\mu(|D\mathbf{y}|) D\mathbf{y},$$

and $\mu(\cdot)$ is given by the Cross model for viscosity described by (3).

Replacing $\mathbf{y}_h$ by its corresponding finite approximation we can write

$$\left(\int_\Omega 2\mu\Big(\Big| \sum_{j=1}^{N_y} y_j D\phi_j \Big| \Big) \sum_{k=1}^{N_y} y_k D\phi_k : \nabla \phi_i \right)_{i=1...N_y} = \mathbf{Q}(Y) \, .$$

Hence system (10) becomes

$$\begin{cases} \mathbf{Q}(Y) + \mathbf{G}(Y) Y + B^T P = F \\ BY = 0 \, . \end{cases} \tag{11}$$

As for the cost function (6), it is also discretized using the FEM basis functions. Assuming that we fix a mesh for the domain Ω, we refer to the

basis functions associated to the nodes in Ω_{part} as $(\phi_i)_{i=1\ldots N_o}$ and to those on Γ_{in}, as $(\phi_i)_{i=1\ldots N_u}$. The approximated control function is then defined by

$$\mathbf{u}_h = \sum_{j=1}^{N_u} u_j \phi_j \, .$$

To discretize the first term we replace both $\mathbf{y}$ and $\mathbf{y}_d$ by their respective finite dimensional approximations $\mathbf{y}_h$ and $\mathbf{y}_{h_d}$ given by

$$\mathbf{y}_{h_d} = \sum_{i=1}^{N_0} y_{d_i} \phi_i \, .$$

We then obtain

$$\begin{aligned}
&\int_{\Omega_{part}} \left\langle \sum_i^{N_o} (y_i - y_{d_i})\phi_i, \sum_j^{N_o} (y_j - y_{d_j})\phi_j \right\rangle dx \\
&= \int_{\Omega_{part}} \sum_i^{N_o} (y_i - y_{d_i}) \sum_j^{N_o} (y_j - y_{d_j}) \left\langle \phi_i, \phi_j \right\rangle \, dx \\
&= \sum_i^{N_o} (y_i - y_{d_i}) \sum_j^{N_o} (y_j - y_{d_j}) \int_{\Omega_{part}} \phi_i \phi_j \, dx \\
&= (Y - Y_d)^T \mathbf{M} (Y - Y_d) = \langle (Y - Y_d), \mathbf{M}(Y - Y_d) \rangle \\
&= (Y - Y_d, Y - Y_d)_M = \|Y - Y_d\|^2_{N_y}
\end{aligned} \tag{12}$$

where $\| \cdot \|_{N_y}$ is the norm induced by the inner product $(\cdot, \cdot)_M$, $Y_d \in R^{N_y}$ is constituted by y_{d_i} in the components corresponding to the observations nodes (N_o) and null in the remaining and $\mathbf{M}$ is a $N_y \times N_y$ matrix where the elements in the observations nodes positions are given by

$$m_{ij} = \int_{\Omega_{part}} \phi_i \phi_j \, dx$$

and the others are also null.

We now turn our attention to the term related to the WSS. From (5) and taking

$$\mathbf{w} = 2\mu(|D\mathbf{y}|)D\mathbf{y}\,\mathbf{n} - [2\mu(|D\mathbf{y}|)(D\mathbf{y}\,\mathbf{n})\cdot\mathbf{n}]\mathbf{n}$$

we get

$$w = \sqrt{\langle \mathbf{w}, \mathbf{w}\rangle}\,.$$

Since w will be evaluated on the no-slip boundary, $D\mathbf{y}$ must be approximated by an expression $D(Y)$ depending on the neighborhood elements where the velocity doesn't vanish. Such expression can be obtained using finite differences or an inheritance based averaging method ([25]). Then the approximation w_h can be writen as

$$w_h(Y) = \sqrt{\langle \mathbf{w}_h(Y), \mathbf{w}_h(Y)\rangle}\,.$$

where

$$\mathbf{w}_h(Y) = 2\mu\left(D(Y)\right)\left(D(Y)\,\mathbf{n} - \left(D(Y)\,\mathbf{n}\cdot\mathbf{n}\right)\mathbf{n}\right).$$

A similar procedure for w_d (WSS) is used to approximate

$$\int\limits_{\Gamma_{wall}} |w - w_d|^2\,dx$$

by

$$\int\limits_{\Gamma_{wall}} \left|w_h - w_{h_d}\right|^2 = \mathbf{W}(Y) \tag{13}$$

where $\mathbf{W}$, obtained by a Gaussian Quadrature rule, depends nonlinearly on Y.

Finally, for the regularization term we have

$$\begin{aligned}
&\int\limits_{\Gamma_{in}} \left|\sum_i^{N_u} u_i\nabla\phi_i\right|^2 dx = \int\limits_{\Gamma_{in}} \left\langle \sum_i^{N_u} u_i\nabla\phi_i, \sum_j^{N_u} u_j\nabla\phi_j \right\rangle dx \\
= &\sum_i^{N_u} u_i \sum_j^{N_u} u_j \int\limits_{\Gamma_{in}} \nabla\phi_i\nabla\phi_j = U^T\mathbf{A}U \\
= &\langle U, \mathbf{A}U\rangle = (U,U)_A = \|U\|^2_{N_u}
\end{aligned} \tag{14}$$

where $\|\cdot\|_{N_u}$ is the norm induced by the inner product $(\cdot,\cdot)_A$ and $\mathbf{A}$ is a symmetric $N_u \times N_u$ matrix where each element is given by

$$a_{ij} = \int_{\Gamma_{in}} \nabla\phi_i \nabla\phi_j \, dx \, .$$

Taking into account (11), (12), (13) and (14), the discrete version of the control problem (6 - 7) becomes

$$J(Y,U) = w_1 \|Y - Y_d\|^2_{N_y} + w_2 \mathbf{W}(Y) + w_3 \|U\|^2_{N_u} \tag{15}$$

subject to

$$\begin{cases} \mathbf{Q}(Y) + \mathbf{G}(Y)Y + B^T P = F \\ BY = 0 \, . \end{cases} \tag{16}$$

The vector $Y = (Y_u, U)$ includes the controlled velocity coefficients U and the uncontrolled ones, represented by $Y_u = Y_u(U)$.

4.1. Sequential Quadratic Programming (SQP)

To solve problem (15 - 16) which is nonlinear both with respect to the cost function and constraints we use a particular Sequential Quadratic Programming (SQP) approach implemented in the package Sparse Nonlinear Optimization (SNOPT) which is briefly described here (see [13, 26] for more details).

First, a major step is required to approximate the nonlinear problem by a quadratic programming problem (QP). The constraints of such approximation correspond to the linearization of (16). The quadratic cost is a second order approximation to the modified Lagrangian function associated to (15 - 16). The Hessian matrix is replaced by a quasi-Newton approximation obtained by a BFGS update. The second step consists in solving the (QP) problem which is done by a reduced-Hessian iterative method implemented in SQOPT ([15]). The solution of the approximation (QP) is used to compute a descent direction for (15 - 16). A line search method is then executed to find the new solution of the nonlinear problem.

The strength of this approach is the fact that it was tested in large scale nonlinear optimization problems with up to 40000 variables (see [13]).

5. Numerical results

As known data y_d and w_d we used synthetic data numerically generated. For this purpose, we consider a 2D stenosed vessel (see Figure 1) with length

equal to $L = 2R$, maximum diameter $D = 2R$ and minimum diameter $d = R$ with $R = 3.1mm$, which is close to physiological measures ([2]). For the fluid model we consider the generalized Cross model, as described in Section 2, with boundary conditions defined in (7). The parameters for the generalized Cross model were chosen as in [2]:

$$\mu_0 = 1.6e^{-1}\, Pa.s, \quad \mu_\infty = 3.6e^{-3}\, Pa.s$$
$$a = 1.23, \quad b = 0.64, \quad \lambda = 8.2\, s$$
$$\rho = 1059\, Kg/m^3\,.$$

To construct and to treat our working domains we resort to COMSOL Multiphysics ([27]). Using the available options for Laminar Flow, we built a mesh composed by 3398 triangular and quadrilateral elements with 15986 degrees of freedom (dofs) for the velocity. Quadrilateral elements were used to refine the mesh along the no-slip boundaries, the regions of boundary layers. The minimum element quality registered was 0.2628 and the average element quality was 0.8262 (note that 0 corresponds to a degenerate element and 1 corresponds to a symmetric element).

The fluid model was solved by imposing a Poiseuille velocity profile at the inlet with a maximum velocity given by $U_0 = 0.0993\, m/s$, which corresponds to the Reynolds number equal to 120. The nonlinear problem was treated with Newton's method while each resulting linear system was solved using the direct solver PARDISO. We used the Nested Dissection Method, as a preordering algorithm, to minimize the zero elements after the factorization. Such methods are also available in COMSOL Multiphysics.

Figure 2 represents the velocity field magnitude obtained as described before, where we highlight the recirculation region that appears downstream the stenosis. We compare the results obtained with the Cross model with those for the Newtonian case where the viscosity is equal to μ_∞. These results are consistent with those obtained in [2], even for a different stenosed vessel.

Figure 3 represents the magnitude of the WSS for the non-Newtonian case. As expected, we observe a high increase of the magnitude value in the region of partial obstruction of the flow, when comparing with the remaining part of the vessel.

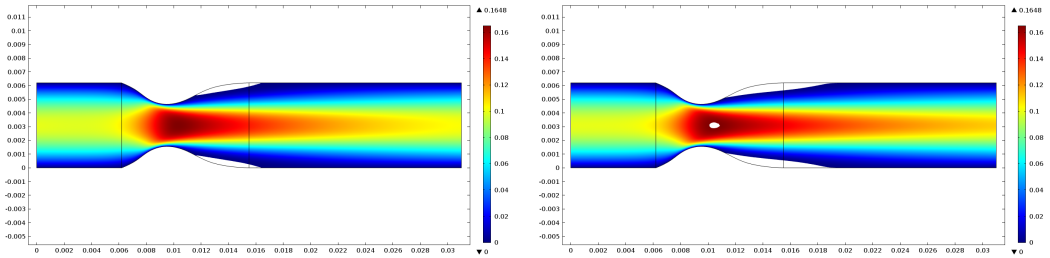

Figure 2: Velocity field magnitude highlighting the recirculation region downstream the stenosis obtained with the direct problem. Left: non-Newtonian case. Right: Newtonian case.

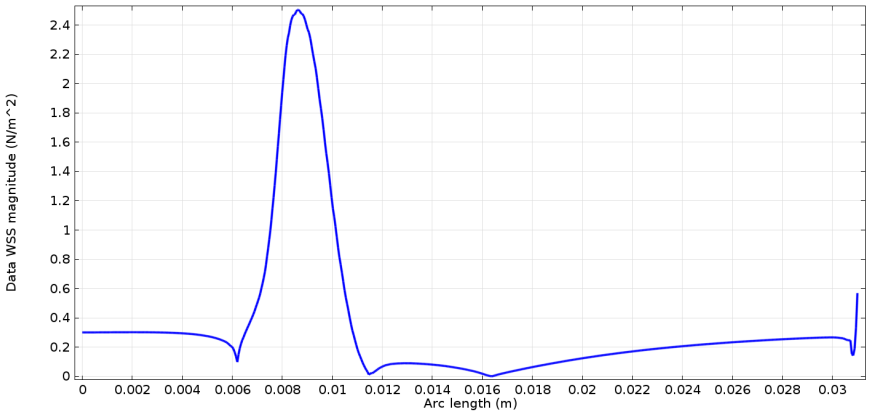

Figure 3: WSS magnitude obtained for the direct problem

5.1. Choice of parameters and validation

The cost function (6) plays an important role in the performance of the DA method. It depends both on the observed domain Ω_{part} and on the weighting parameters w_1, w_2 and w_3. The correct choice of the observed domain is an important issue (see [3]). It has been considered for the discrete linearized Navier-Stokes equations in [9], where Ω_{part} was taken as a finite number of points. Here we don't deal with this issue, and we assume that $\mathbf{y}_d = \mathbf{y}_d(x, y)$ is fully determined over Ω_{part}, corresponding to the vertical blue lines represented in Figure 1. We will be concerned, however, with the choice of the weighting parameters for the cost function.

It is well known that a proper balance of the terms in a quadratic type cost function ($w_2 = 0$) can be treated by Tikhonov's regularization techniques (see

[9] for some applications). But, as far as we know, such techniques cannot be easily applied to a nonlinear cost function like (15). Therefore, we present an heuristic numerical study to investigate which set of parameters (w_1, w_2, w_3) provides a better approximation of the data, including the velocity, the WSS and the inlet profile, through the optimal control variable.

In order to solve each problem of type (15 - 16) we use the SQP method implemented in SNOPT, as briefly described in Section 4.1. To compute the gradient of the cost function with respect to the control variables we used the adjoint method ([25]). The optimality tolerance, which determines the accuracy of the approximation of first-order optimality conditions ([14]), was fixed to 10^{-6}. For the QP solver, we imposed that the Cholesky factor of the reduced Hessian should be kept. The control problems were solved using the mesh described above and taking 37 degrees of freedom for the control variable imposed on the inlet boundary.

Table 1: Values of the cost function parameters for fixed w_2 and w_3 and varying w_1.

	$\int_{\Omega_{part}} \lvert Y\rvert^2$	$\int_{\Gamma_{wall}} \lvert W\rvert^2$	$\int_{\Gamma_{in}} \lvert\nabla \mathbf{u}\rvert^2$	CF
$(0, 10^6, 10^{-3})$	4.152000×10^{-7}	1.838053×10^{-13}	8.190109	0.0081902934
$(10^5, 10^6, 10^{-3})$	2.049161×10^{-11}	2.284326×10^{-16}	8.477968	0.0084800177
$(10^6, 10^6, 10^{-3})$	2.196835×10^{-13}	6.982916×10^{-18}	8.481701	0.0084819206
$(10^7, 10^6, 10^{-3})$	2.225967×10^{-15}	1.029709×10^{-19}	8.482097	0.0084821196

Table 2: Values of the cost function parameters for fixed w_1 and w_3 and varying w_2.

	$\int_{\Omega_{part}} \lvert Y\rvert^2$	$\int_{\Gamma_{wall}} \lvert W\rvert^2$	$\int_{\Gamma_{in}} \lvert\nabla \mathbf{u}\rvert^2$	CF
$(10^6, 0, 10^{-3})$	2.229353×10^{-13}	4.493504×10^{-13}	8.481696	0.0084819189
$(10^6, 10^5, 10^{-3})$	2.198003×10^{-13}	6.444382×10^{-16}	8.481701	0.0084819206
$(10^6, 10^7, 10^{-3})$	2.196719×10^{-13}	7.027137×10^{-20}	8.481701	0.0084819206

Table 3: Values of the cost function parameters for fixed w_1 and w_2 and varying w_3.

	$\int_{\Omega_{part}} \lvert Y\rvert^2$	$\int_{\Gamma_{wall}} \lvert W\rvert^2$	$\int_{\Gamma_{in}} \lvert\nabla \mathbf{u}\rvert^2$	CF
$(10^6, 10^6, 10^{-5})$	7.794634×10^{-14}	1.479646×10^{-16}	8.529495	$8.53730414 \times 10^{-5}$
$(10^6, 10^6, 10^{-4})$	2.224927×10^{-15}	1.898105×10^{-21}	8.482097	$8.48211969 \times 10^{-4}$
$(10^6, 10^6, 10^{-2})$	2.052022×10^{-11}	2.194004×10^{-14}	8.477961	0.0848001567
$(10^6, 10^6, 10^{-1})$	1.727427×10^{-9}	2.725338×10^{-11}	8.445729	0.8463276594
$(10^6, 10^6, 0)$	6.029549×10^{-14}	9.237606×10^{-17}	171.890855	$6.03878696 \times 10^{-8}$
$(10^6, 10^6, 10^1)$	4.600914×10^{-6}	3.811922×10^{-6}	6.645082	74.863651813

We can observe the quantitative results obtained in the simulations in the tables 1, 2 and 3, where we take $Y = \mathbf{y} - \mathbf{y}_d$, $W = w - w_d$ and CF to represent the final cost function value. We can check that both the velocity and the WSS are better approximated when all the parameters are non null.

As expected, in Table 1 we notice that better results for the velocity field and WSS are attained when w_1 increases. Such behavior of w_1 requires a growing number of SNOPT iterations to solve (15 - 16). Therefore, we only present results obtained for less than 400 iterations. If we consider $w_1 = 0$, the resulting cost function has the worst performance for the velocity field approximation and one of the worst for WSS. Maintaining w_1 and w_3 and increasing w_2, in Table 2 we observe better results for WSS and also for the velocity field, but less evident. We conclude that the existence of the term $\int_{\Omega_{part}} |\mathbf{y} - \mathbf{y}_d|^2$ is crucial for good velocity and WSS approximations. We also observed that better results are obtained when the term $\int_{\Gamma_{wall}} |w - w_d|^2$ is present in the cost function.

Let us now consider the so called regularization term $\int_{\Gamma_{in}} |\nabla \mathbf{u}|^2$. By observing Table 3, it is clear that the cost function value is highly affected by this term, as we can see when we change the value of w_3, maintaining w_1 and w_2. We can also observe that if $w_3 = 0$ we have good approximations for the velocity field and WSS, once the minimization only concerns the remaining terms. However, the absence of a regularization term may possibly induce a

spurious minimum (see for instance [3]). This is the case here as we can confirm in Figure 5, observing the results on the right hand side. The optimal control for $w_3 = 0$ is highly irregular and far from the parabolic profile. Thus, although it corresponds to a minimum for the discrete control problem, it does not represent an admissible control function for our DA problem.

Looking at the three tables we conclude that, within the tests we have considered (less than 400 SNOPT total iterations), the set of parameters corresponding to better approximations is $(10^7, 10^7, 10^{-3})$. However we need 381 iterations to find the optimal solution, which corresponds to a large computation time. To set a reasonable balance between accuracy and computational effort, and since the weights

$$(w_1, w_2, w_3) = (10^6, 10^6, 10^{-3}) \tag{17}$$

also perform very well, while taking only 281 iterations to minimize, we set these values as our reference choice for the DA problem. Therefore, in the remainder, we will focus in showing how the set of parameters (17) can perform better than the limit cases, when one of the weights vanishes. This is the purpose of figures 4 and 5 where we represent the optimal controls versus the inlet profile used to generate $\mathbf{y}_d$.

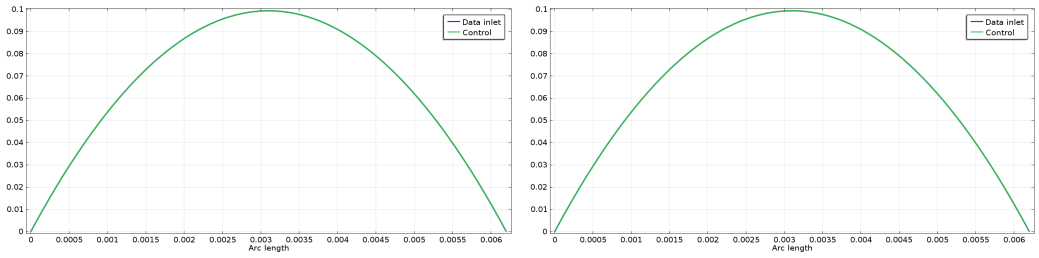

Figure 4: Left: control for $(10^6, 10^6, 10^{-3})$. Right: control for $(10^6, 0, 10^{-3})$.

To compare the effect of the different choices of parameters, not only in the minimization of each term, but in the quality of the velocity approximation, we also report in Table 4 both relative and absolute errors given by

$$R_e = \frac{\|\mathbf{y} - \mathbf{y}_d\|_2}{\|\mathbf{y}_d\|_2} \quad \text{and} \quad A_e = \|\mathbf{y} - \mathbf{y}_d\|_2,$$

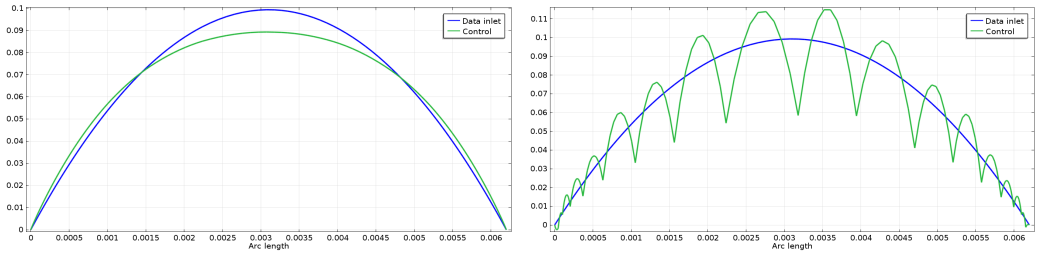

Figure 5: Left: control for $(0, 10^6, 10^{-3})$. Right: control for $(10^6, 10^6, 0)$.

where $\|\cdot\|_2$ is the $\mathbf{L}^2$-norm.

Table 4: Relative and absolute errors for different parameters computed in Ω_{part}.

Errors	$(0, 10^6, 10^{-3})$	$(10^6, 10^6, 10^{-3})$	$(10^6, 0, 10^{-3})$	$(10^6, 10^6, 0)$
R_e	0.037254	2.709809×10^{-5}	2.729791×10^{-5}	1.419653×10^{-5}
A_e	6.443602×10^{-4}	4.687041×10^{-7}	4.721603×10^{-7}	2.455514×10^{-7}

We can easily confirm that the worst cost function is the one for which the velocity term is missing, and that it is better to have the WSS term than not having it.

We conclude that solving the control problem with (17) is the best option, within a certain computational effort limit. To illustrate, we represent in figures 6 - 10 the velocity, the pressure, and the WSS magnitude corresponding to the optimal solution. We compare these results with the solution from which we took the observations y_d and w_d.

We can see, from these results, that the original solution was perfectly reconstructed from the observations.

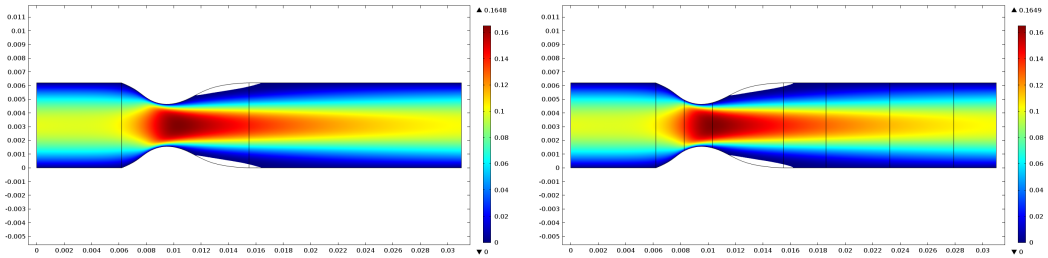

Figure 6: Left: velocity field of the direct problem highlighting the recirculation region. Right: velocity field of the controlled problem highlighting the recirculation region

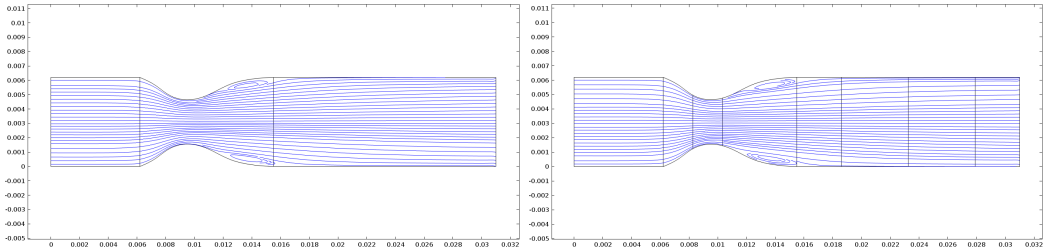

Figure 7: Leff: velocity streamlines of the direct problem. Right: velocity streamlines of the controlled problem

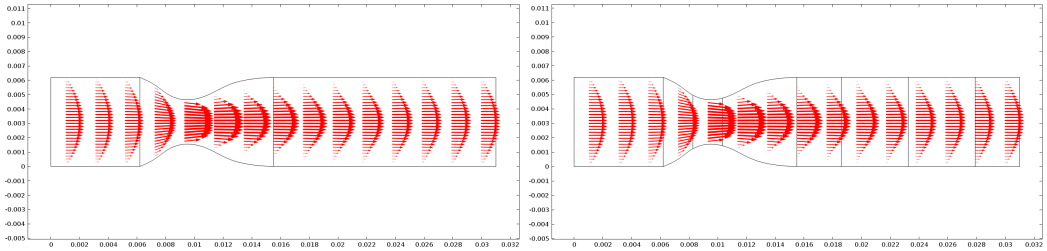

Figure 8: Leff: velocity field profile of the direct problem. Right: velocity field profile of the controlled problem

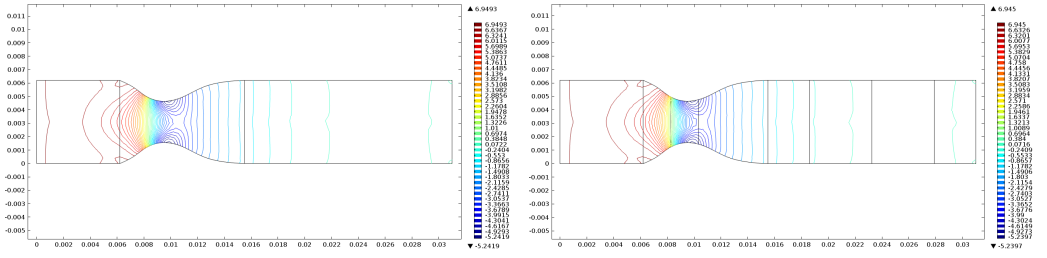

Figure 9: Leff: pressure contour of the direct problem. Right: pressure contour of the controlled problem

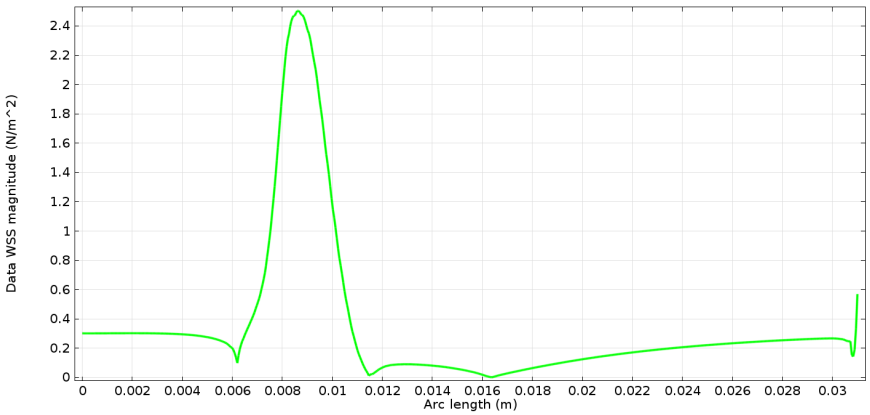

Figure 10: WSS magnitude obtained with the controlled problem

5.2. Robustness of the parameters

In this section we show the robustness of the proposed parameters given by (17) in the DA method, with respect to different velocity field inlet profiles and to different stenosis degrees.

5.2.1. Robustness to data inlet profile

We obtained different data using a Power-Law inlet profile (see [20]) given by

$$\frac{\xi+2}{\xi}U_1\left(1-\left(\frac{y-R}{R}\right)^{\xi}\right). \tag{18}$$

Note that, for $\xi = 2$, expression (18) gives the particular case of Poiseuille flow. In our simulations we have considered $\xi = 4$ and $\xi = 9$ with profiles represented in Figure 11. Constant U_1 was chosen in such a way that the Reynolds number is equal to 120, as above. We tested $\xi = 9$ which is commonly considered in the simulations of blood flow in arteries [20], and $\xi = 4$ which is an intermediate value between 2 and 9.

Like in the previous section we compare the set of parameters (17) with the limit cases. The quantitative results are those reported in tables 5 and 6. Similar conclusions can be inferred for both profiles. The importance of the WSS term in the cost function is more expressive when compared with

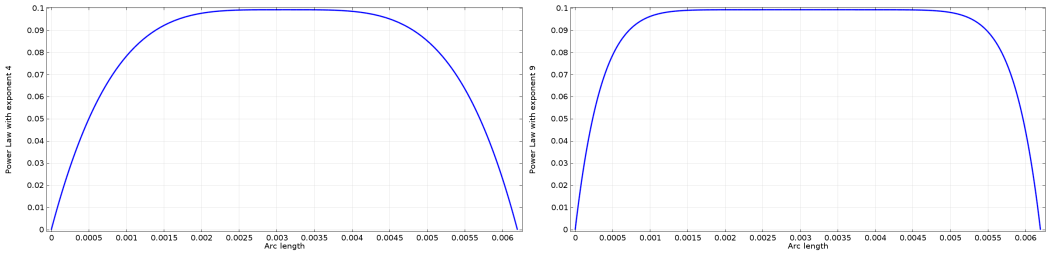

Figure 11: Power Law velocity field inlet profile (18):left: with exponent 4; right: with exponent 9.

the parabolic profile. To confirm these conclusions, see tables 7 and 8 where relative and absolute errors are compared.

Table 5: Results for the Power-Law velocity field inlet profile (18), with exponent 4.

$\xi = 4$	$\int_{\Omega_{part}} \lvert Y\rvert^2$	$\int_{\Gamma_{wall}} \lvert W\rvert^2$	$\int_{\Gamma_{in}} \lvert\nabla \mathbf{u}\rvert^2$	CF
$(0, 10^6, 10^{-3})$	1.017793×10^{-6}	2.595413×10^{-13}	13.747798	0.0137480578
$(10^6, 10^6, 10^{-3})$	2.083886×10^{-12}	1.033918×10^{-12}	14.513515	0.0145166331
$(10^6, 0, 10^{-3})$	7.946703×10^{-11}	7.098585×10^{-8}	14.168067	0.0142475338
$(10^6, 10^6, 0)$	6.535708×10^{-12}	1.204306×10^{-11}	392.3837	$1.8578771535 \times 10^{-5}$

Table 6: Results for the Power-Law velocity field inlet profile (18), with exponent 9.

$\xi = 9$	$\int_{\Omega_{part}} \lvert Y\rvert^2$	$\int_{\Gamma_{wall}} \lvert W\rvert^2$	$\int_{\Gamma_{in}} \lvert\nabla \mathbf{u}\rvert^2$	CF
$(0, 10^6, 10^{-3})$	1.001349×10^{-5}	3.259272×10^{-13}	20.106642	0.020106968
$(10^6, 10^6, 10^{-3})$	7.801032×10^{-11}	2.094571×10^{-11}	29.855718	0.0299546736
$(10^6, 0, 10^{-3})$	7.960777×10^{-10}	1.294974×10^{-6}	24.151194	0.0249472714
$(10^6, 10^6, 0)$	1.582331×10^{-15}	7.475844×10^{-22}	565.871393	1.582331×10^{-9}

Table 7: Relative and absolute errors for exponent 4, computed in Ω_{part}.

$\xi = 4$	$(0, 10^6, 10^{-3})$	$(10^6, 10^6, 10^{-3})$	$(10^6, 0, 10^{-3})$	$(10^6, 10^6, 0)$
R_e	0.048416	6.927796×10^{-5}	4.278107×10^{-4}	1.226887×10^{-4}
A_e	0.001009	1.443567×10^{-6}	8.914428×10^{-6}	2.556503×10^{-6}

Table 8: Relative and absolute errors for exponent 9, computed in Ω_{part}.

$\xi = 9$	$(0, 10^6, 10^{-3})$	$(10^6, 10^6, 10^{-3})$	$(10^6, 0, 10^{-3})$	$(10^6, 10^6, 0)$
R_e	0.134635	3.757856×10^{-4}	0.0012	1.692438×10^{-6}
A_e	0.003164	8.832345×10^{-6}	2.821485×10^{-5}	3.977852×10^{-8}

Furthermore, the only cost function that provides an adjustment of the control function with the original inlet profile, is precisely the one defined by (17). We can also see that such adjustment is less precise for $\xi = 9$. Figures 12 and 13 illustrate these conclusions. They show the adjustment of the control function, for each inlet profile, computed with the different sets of parameters described above.

Finally, in Table 9 we compare the errors for the different velocity field inlet profiles, obtained with the choice of parameters (17). We observe that the DA problem solved with any of the three inlet conditions gives good approximations of the velocity field.

Nevertheless, the closer we are to the Poiseuille inlet profile, the better relative and absolute errors are obtained.

5.2.2. Robustness as a function of the stenosis degree

In this section we compare the control problem solutions obtained for the cost function with parameters (17) in four geometries, three stenosed

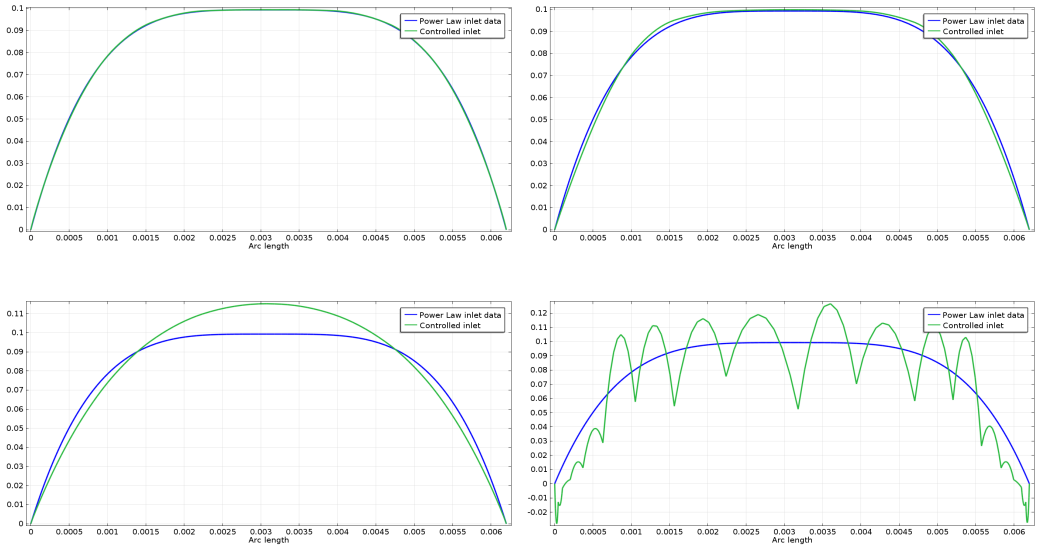

Figure 12: Power Law velocity field inlet profile with exponent 4; upper left corner: $(10^6, 10^6, 10^{-3})$, upper right corner: $(10^6, 0, 10^{-3})$, bottom left corner: $(0, 10^6, 10^{-3})$, bottom right corner $(10^6, 10^6, 0)$.

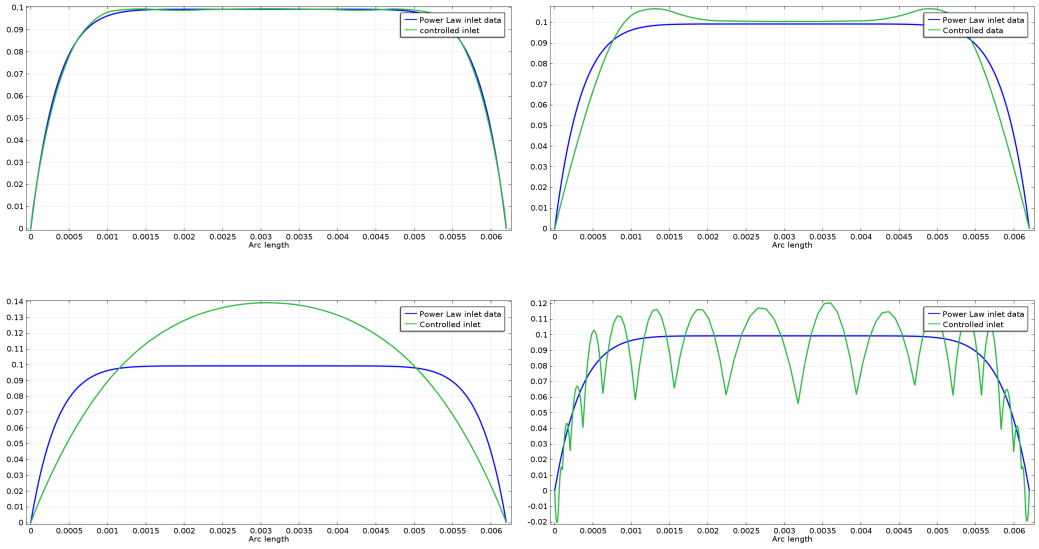

Figure 13: Power Law velocity field inlet profile with exponent 9; upper left corner: $(10^6, 10^6, 10^{-3})$, upper right corner: $(10^6, 0, 10^{-3})$, bottom left corner: $(0, 10^6, 10^{-3})$, bottom right corner $(10^6, 10^6, 0)$.

Table 9: Relative and absolute errors for different inlet profiles, computed with the set of parameters (17) in Ω_{part}.

Errors	Poiseuille	Power-Law $\xi = 4$	Power-Law $\xi = 9$
R_e	2.709809×10^{-5}	6.927796×10^{-5}	3.757856×10^{-4}
A_e	4.687041×10^{-7}	1.443567×10^{-6}	8.832345×10^{-6}

channels with different degrees and a straight channel. The four geometries are represented in Figure 14.

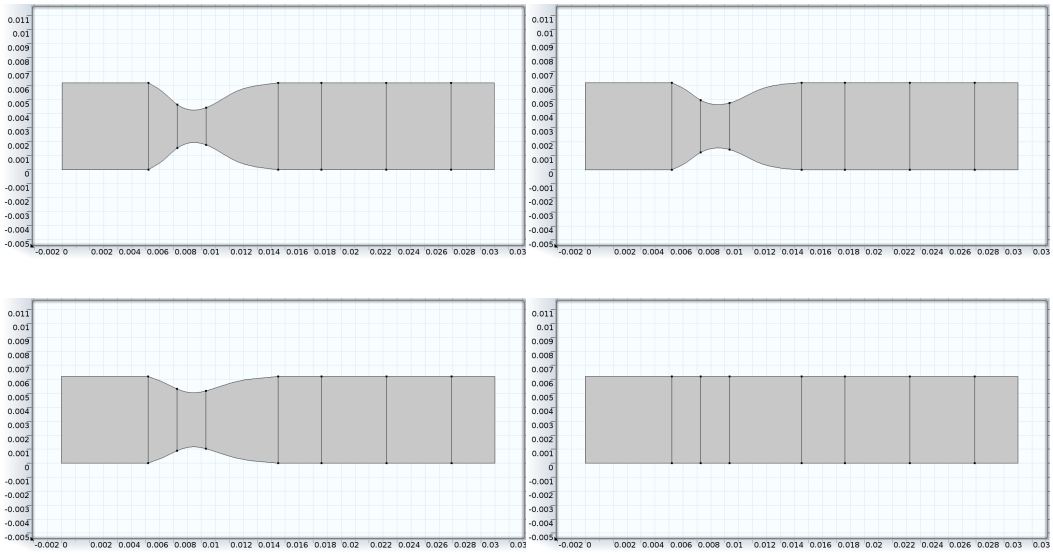

Figure 14: Upper leff corner: stenosis with $d = 3R/4$. Upper right corner: stenosis with $d = R$. Bottom left corner: stenosis with $d = 5R/4$. Bottom right corner: straight channel. In all cases $L = 10R$ and $D = 2R$. Dofs for velocity: about 10000.

The aim of this study is to show that our choice of parameters given by (17) obtained in the Section 5.1 is robust with respect to the changes imposed in the different geometries. In fact, even changing the geometry, we can see that a numerical solution for optimal control problem can be found, and that the original velocity is very well approximated, as shown by the relative and absolute errors in Table 10.

Table 10: Comparison between three different stenosis and a straight channel, regarding the cost function value, as well as the relative R_e and absolute A_e errors computed in Ω_{part}.

Values	Stenosis $d = 3R/4$	Stenosis $d = R$	Stenosis $d = 5R/4$	Channel
CF	0.0084819835	0.0084819208	0.0084818721	0.0084818125
R_e	2.068563×10^{-5}	2.709878×10^{-5}	3.19736×10^{-5}	3.803092×10^{-5}
A_e	3.960592×10^{-7}	4.687051×10^{-7}	5.176455×10^{-7}	5.703546×10^{-7}

5.3. Effect of noise filtering

In this section we study the effect of our DA method in filtering the noise that can be added to the observed data y_d. In real applications this can be due to many different reasons, such as the lack of accuracy of the observation devices or to intrinsic errors of the model. Here noise samples were generated in a random way, normally distributed, with zero mean and standard deviation equal to $\bar{\sigma}_1 = 0.05\frac{U_0}{3}$, $\bar{\sigma}_2 = 0.1\frac{U_0}{3}$ and $\bar{\sigma}_3 = 0.2\frac{U_0}{3}$, respectively. For the data we use the reference stenosis geometry with radius and the velocity profile as described in Figure 2 (non-Newtonian case). However we include also in Ω_{part} the inlet boundary.

To understand the filtering effect of the formulation (15 - 16) we compare the solution obtained with our reference set of parameters (17) with a direct approach. This approach consists in obtaining the numerical solution of the non-Newtonian model (1), by using a noisy parabolic profile, as inlet boundary condition. Such technique can be seen as the computational least expensive filtering technique, when we wish to recover the solution downstream the observations. We remark, however, that it could not be used if we pretended to reconstruct the solution upstream the observed data. A similar comparison was done in [10] for the Navier-Stokes equations.

The differences between the solutions obtained by noise filtering, using both methods, is presented in the Table 11. As an index of precision, we computed a posteriori, the relative error R_e and the absolute error A_e in the entire domain.

The conclusions we have for the non-Newtonian problems are similar to those obtained in [10] for the Newtonian problem.

We can observe, as expected, that higher values for noise correspond to worst values for R_e and A_e

Table 11: Comparison between relative and absolute errors computed in Ω for the controlled problem (CP) and the direct problem (DP) with different noise.

Noise	Problem type	R_e	A_e
$\bar{\sigma} = 0.05\frac{U_0}{3}$	CP	0.001968	$2.193509e^{-6}$
	DP	0.004606	$5.134504e^{-6}$
$\bar{\sigma} = 0.1\frac{U_0}{3}$	CP	0.004974	$5.545074e^{-6}$
	DP	0.009214	$1.027040e^{-5}$
$\bar{\sigma} = 0.2\frac{U_0}{3}$	CP	0.009164	$1.021493e^{-5}$
	DP	0.018324	$2.049306e^{-5}$

6. Conclusion

In this work we proposed a DA method based on a variational approach to numerically reconstruct non-Newtonian blood flow behavior on different bidimensional geometries.

We introduced a new cost function which takes into account the role of the WSS in the optimization process and we concluded, by testing the parameters w_1, w_2 and w_3, that this modification provides better results for both the velocity field and the WSS. The importance of the presence of a regularization term in the cost function was also tested. We observed that the absence of this term gives a completely irregular control corresponding to a spurious minimum. We also proposed a set of parameters as a reasonable choice when balancing the approximation accuracy and the computational effort.

The method was validated by testing the robustness with respect to changes in the geometry as well as to different inlet profiles. In each one of the cases the cost function was minimized and we obtained very good approximations for the velocity field and the WSS.

Finally, we tested our method as a noise filter adding three different amounts of noise to the data solution, including the inlet boundary and we compared with the Direct filtering method, where the noise is added to the inlet boundary condition. The conclusions are consistent with the results

obtained in [10] for the Newtonian case. A DA approach gives better results in correcting the noisy measurements than a Direct approach.

Acknowledgments This work has been partially supported by FCT (Portugal) through the Research Centers CMA/FCT/UNL, CEMAT-IST, grant SFRH/BPD/66638/2009 and the projects PTDC/MAT109973/2009 and EXCL/MAT-NAN/0114/2012.

[1] N. Arada, Optimal control of shear-thinning fluids, SIAM J. Control Optim., 50 (4) (2012) 2515-2542.

[2] T. Bodnar, A. Sequeira and M. Prosi, On the shear-thinning and viscoelastic effects of blood flow under various flow rates, Appl. Math. Comput., Elsevier, 217 (2011) 5055-5067.

[3] J. Burkardt, M. Gunzburger, J. Peterson, Insensitivite Functionals, Inconsistent Gradients, Spurious Minima and Regularized Funcionals in Flow Optimization Problems, Int. J. Comput. Fluid Dyn., 16 (3) 2002) 171-185.

[4] V. Calvez, J. G. Houot, N. Meunier, A. Raoult and G. Rusnakova. Mathematical and Numerical Model or Early Atherosclerosis Lesions, ESAIM: PROC., 30 (2010) 1-14.

[5] E. Casas, L.A. Fernandez, Boundary control of quasilinear elliptic equations, Rapport de Recherche, INRIA, 782 (1988).

[6] E. Casas, L.A. Fernandez, Distributed control of systems governed by a general class of quasilinear elliptic equations, J. Differ. Equ., 104 (1993) 20-47.

[7] J. R. Cebral, M. A. Castro, J. E. Burgess, R. S. Pergolizzi, M. J. Sheridan and C. M. Putman, Characterization of cerebral aneurysms for assessing risk of rupture by using patient-specific computational hemodynamics models, Am. J. Neuroradiol., 26 (2005) 2550-2559.

[8] M. J. Crochet, A. R. Davies, K. Walters, Numerical Simulation of Non-Newtonian Flow, first ed., Elsevier Science Publishers B.V., New York, 1984.

[9] M. D' Elia, M. Perego, A. Veneziani, A Variational Data Assimilation Procedure for the Incompressible Navier-Stokes Equations in Hemodynamics, J. Sci. Comput., 52 (2) (2011) 340-359.

[10] M. D' Elia, A. Veneziani, A Data Assimilation technique for including noisy measurements of the velocity field into Navier-Stokes simulations, Proc. of V European Conference on Computational Fluid Dynamics, ECCOMAS, (2010).

[11] M. D'Elia, A. Veneziani, Methods for assimilating blood velocity measures in hemodynamics simulations: preliminary results, Procedia Comput. Sci., 1 (1) (2010) 1225-1233.

[12] A. Garambuto, J. Janela, A. Moura and A. Sequeira, Sensitivity of hemodynamics in a patient specific cerebral aneurysm to vascular geometry and blood rheology, Math. Biosci. Eng., 8 (2) (2011) 409-423.

[13] P. Gill, W. Murray, M.A. Saunders, SNOPT: An SQP Algoritm for Large-Scale Constrained Optimization, Soc. for Industrial and Appl. Math., SIAM REVIEW, 47 (2005) 99-131.

[14] P. Gill, W. Murray, M.A. Saunders User's guide for SNOPT Version 7: Software for Large-Scale Nonlinear Programming, 2008.

[15] P. Gill, W. Murray, M.A. Saunders, User's guide for SQOPT Version 7: Software for large-scale linear and quadratic programming, Numerical Analysis Report 06-1, Department of Mathematics, University of California San Diego, La Jolla, CA, 2006.

[16] T. Guerra, Distributed control for shear-thinning non-Newtonian fluids, J. Math. Fluid Mech., 14 (4)(2012) 771-789.

[17] M. Gunzburger, Adjoint Equation-Based Methods for Control Problems in Incompressible, Viscous Flows, Flow, Turbul. and Combust., 65 (3) (2000) 249-272.

[18] M. Gunzburger, C. Trenchea, Analysis of an optimal control problem for the three-dimensional coupled modified Navier-Stokes and Maxwell equations, J. Math. Anal. Appl., 333 (2007) 295-310.

[19] H. Meng, Z. Wang, Y. Hoi, L. Gao, E. Metaxa, D. D. Swartz and J. Kolega, Complex hemodynamics at the apex of an arterial bifurcation induces vascular remodeling resembling cerebral aneurysm initiation, Stroke, 38 (2007) 1924-1931.

[20] A. Quarteroni, L. Formaggia, Mathematical Modelling and Numerical Simulation of the Cardiovascular System, Modelling of living Systems, Handbook of Numererical Analysis Series, Elsevier, Amesterdam, 2002.

[21] A. M. Robertson, A. Sequeira, G. R. Owens, Rheological models for blood, in: Cardiovascular Mathematics, Modeling and Simulation of the circulatory system, Springer, Milan, 1, 2009, pp. 211-241.

[22] T. Slawig, Distributed control for a class of non-Newtonian fluids, J. Differ. Equ., 219 (2005) 116-143.

[23] D. Wachsmuth, T. Roubíček, Optimal control of incompressible non-Newtonian fluids, Z. Anal. Anwend, 29 (2010) 351-376.

[24] K. Yeleswarapu, M. Kamaneva K.R. Rajagopal and J.F. Antaki, The flow of blood in tubes-theory and experiment, Mech. Res. Commun., 25 (1998) 257-262.

[25] *COMSOL Multiphysics, Users Guide*, COMSOL 4.3, 2012.

[26] *Optimization Module, Users Guide*, COMSOL 4.3, 2012.

[27] *COMSOL Multiphysics, http://www.comsol.com.*